Research Article | Vol. 10, No. 2 | 1 Feb 2019 | BIOMEDICAL OPTICS EXPRESS 500
Biomedical Optics EXPRESS

Label-free detection of hydrogen peroxide-induced oxidative stress in human retinal pigment epithelium cells via laser tweezers Raman spectroscopy

YANG CHEN,[1] ZHIQIANG WANG,[2] YAN HUANG,[2,*] SHANGYUAN FENG,[3] ZUCI ZHENG,[3] XIUJIE LIU,[3] AND MENGMENG LIU[3]

[1]*Department of Laboratory Medicine, Fujian Medical University, Fuzhou 350004, China*
[2]*Department of Ophthalmology & Optometry, Fujian Medical University, Fuzhou 350004, China*
[3]*Key Laboratory of Optoelectronic Science and Technology for Medicine, Ministry of Education, Fujian Normal University, Fuzhou 350007, China*
[*]*fjhyan-1988@fjmu.edu.cn*

Abstract: Human retinal pigment epithelium cells under hydrogen peroxide-induced oxidative stress and a ligustrazine-based protective effect were investigated using laser tweezers Raman spectroscopy. Protein and lipid were significantly affected by oxidative damage, along with increased reactive oxygen species (ROS) level within cells. The effects of ligustrazine against the reaction of ROS with protein seemed to be able to inhibit such damages but were limited during the desamidization of amides, along with additional effect on nucleic acid base and DNA phosphoric acid skeleton. This work laid the basis for both understanding the molecular mechanisms of oxidative stress-induced injury and highlighting possible biomarkers in retinal diseases.

1. Introduction

Retinal pigment epithelium (RPE) is a monolayer of pigmented cells located between the retina and the choroid in the eye. As a critical component of blood retinal barrier, RPE transports nutrients and metabolites to the outer retina and photoreceptors through the microvascular bed. Lights focused by the lens are absorbed by the retina and the damaging part may be filtered to keep retinal homeostasis [1,2]. To achieve a good vision, the RPE also plays important roles in nourishing the retina and maintaining fitness and function of photoreceptors, since the RPE could supplement the 11-cis-retinal chromophore to photoreceptors, and phagocytize damaged (photo-oxidized) outer segments of photoreceptors [3]. However, the RPE is not able to renew itself after differentiation. RPE cells are very susceptible to oxidative damage during human life. Oxidative stress usually occurs when there is an imbalance of biological process between production and scavenging mechanism of reactive oxygen species (ROS) in cells [4]. When cells are exposed to oxidative stress, abnormal proteins and lipids accumulate and will further weaken the ability of cellular self-repair, resulting in cell loss [5]. In the retina, the photoreceptor is continuously exposed to light and oxygen, therefore it is particularly susceptible to oxidative stress. Meanwhile, the RPE cells are essential for phagocytosis via the photoreceptor outer segment membrane which is critical for photoreceptor survival, function and renewal. Due to oxidative stress or other stresses, the RPE degeneration usually causes secondary photoreceptor cell death [6]. Given this, oxidative stress to RPE is considered as one of the major causes of eye diseases, such as age-related macular degeneration and diabetic retinopathy [7,8]. As a major factor implicated in the free-radical theory of aging, there are evidences that hydrogen peroxide will induce oxidative stress apoptosis in RPE cells [9–11]. So far, due to the low accumulation of ROS in early oxidative stress, the early detection of oxidative stress in RPE cells remains

#349051 https://doi.org/10.1364/BOE.10.000500
Journal © 2019 Received 23 Oct 2018; revised 11 Dec 2018; accepted 17 Dec 2018; published 9 Jan 2019

Biomedical Optics EXPRESS

difficulties, and the underlying mechanism is still unclear. There are also reports about the protective effects of ligustrazine [12,13]. Many techniques have been proposed for the detection and analysis of in vitro interactions among cells and their environment, such as optical, biochemical, immunochemical and molecular techniques. Since RPE cells are arranged as single layer in vivo, it is important to explore a method that can detect single living cells. However, most of those techniques are invasive and often require preparation steps such as fixation, staining or labeling [14]. Despite of specific biomarker expression in the cells, such methods are not feasible for the study of single living cells. For this reason, there is a need to construct effective strategies from cellular level for monitoring oxidative damage and therapeutic evaluation.

Based on inelastic scattering, Raman spectroscopy (RS) may provide cellular and subcellular information of molecular vibration via a noninvasive and nondestructive way that does not require special labeling or preparation [15]. Compared to traditional spectral methods like infrared spectroscopy, the RS is less influenced by water, which makes it very suitable for biological samples in a water-based environment, ranging from bio fluids, tissue and cells to subcellular components [16,17]. By combining various statistical methods, normal and abnormal cells and tissues can be initially characterized. For instance, classifications of normal and cancerous cell lines from human prostatic, breast, thyroid, and leukemia cells have been successfully classified [18–20]. Recently, a new method derived from RS, called laser tweezers Raman spectroscopy (LTRS), has proven to be a powerful spectroscopic technique for the analysis of individual biological cells in suspension, helping to take Raman analysis of biological samples beyond whole tissue and bulk cells down to the single cell level. The combination of laser tweezers and RS facilitates the whole detection procedure. In addition, when associated with the optical trapping technique, which immobilizes a floating object within the laser focus, interrogation of individual cells is simplified.

Recent studies have shown that LTRS is a promising technique for single cell detection [21]. The nondestructive and noninvasive nature of LTRS allowed performing analysis on live cells, and it minimized prior sample preparation procedures. Ahlawat and colleagues have utilized LTRS for label-free analysis of human colon adenocarcinoma cell cycle synchronized in G0/G1 and G2/M phases via DNA band as an indicator of content in nucleus [22]. Also, the LTRS was successfully used for single cancer cell detection, and the cancer groups could be accurately discriminated from the normal cells based on characteristic Raman signals generated from DNA/RNA and proteins or attributed to effects of cell preparation [21,23,24]. Thus, it may have the potential to use LTRS to examine the effects of oxidative stress and the corresponding oxidation resistant reagent.

In this work, the effects of oxidative stress and relative resistant reagent for human RPE cell were performed by LTRS method. We aimed to preliminarily understand the molecular mechanisms and determine characteristic differences for cellular oxidative stress. This is the first time to investigate the spectral characterization of human RPE cells and the underlying oxidative mechanism by combining LTRS and multivariate methods.

2. Material and methods

2.1. Cell line and culture condition

Human RPE cell line (Jennio Biotech, Guangzhou, China) was cultured in Dulbecco's modified eagle medium (DMEM) supplemented with 1% streptomycin, 1% penicillin, and 10% fetal bovine serum (FBS) (Hyclone, GE Lifescience, USA). Cells were grown in an incubator humidified 5% CO_2 atmosphere at 37°C. Fresh stock of cells was seeded in 9 identical flasks. In this experiment, hydrogen peroxide and ligustrazine were added to the medium of RPE cells to construct models of oxidative stress and asses the protective effect. Cells were divided into three groups and the concentrations of those reagents were determined by referring to previous reports and the concentration gradient experiment

Biomedical Optics EXPRESS

[25,26]. As a result, hydrogen peroxide and ligustrazine with concentrations of 0 μmol/mL and 0 μmol/mL, 200 μmol/mL and 0 μmol/mL, and 200 μmol/mL and 200 μmol/mL were considered as groups of control, oxidative stress, and protective effect, respectively. Cells in logarithmic growth phase were washed twice with phosphate buffer saline (PBS), and then digested by trypsin solution for following steps.

2.2 Cell viability and ROS measurement

Before cell viability measurement, five concentration gradients of cell suspension were set to screen optimum concentration. As a result, 100 μL of cell suspension with number of approximately 5000/μL from each flask was selected and seeded in a 96-well plate, 3 replicates per flask beside 3 blank controls. After 24-hour culture, sample in each well was washed twice with PBS, and the mixture of fresh medium and CCK-8 reagent (Beyotime Biotech, Shanghai, China) under volume ratio of 10:1 was added to each well. After two hours of incubation, cell viability measurement was performed on a MultiskanGO (Thermo, USA) microplate reader. The absorbance and optical density (OD) value were measured under a wavelength of 450 nm that indirectly reflected the number of viable cells. The cell number of each well was calculated according to relative absorbance and the OD value. The 2',7'-dichlorodihydrofluorescein diacetate (H2DCFDA) is a vital fluorescent probe that enters in cells and can be oxidized by ROS, particularly by hydrogen peroxide (H_2O_2) and hydroxyl radicals, yielding the fluorescent product (DCF). This probe is not an equilibrium sensor that can continuously monitor the level of ROS, but it traps or otherwise reacts with ROS. Increasing intracellular ROS to a sufficiently high level would trigger cell death, and thus it was suggested that ROS could be biochemical mediators of apoptosis [27]. Intracellular ROS generation was monitored by fluorescence microscopy, using fluorescence produced from 2',7'-dichlorofluorescein (DCF) after being oxidized from DCFH-DA (Molecular Probes). In brief, RPE cells were incubated with 5 μM DCFH-DA 30 min at 37°C in the dark. Then the cells were washed twice with PBS and cultured in DMEM containing 5% FBS [28]. Fluorescence intensity was determined using a fluorescence microscopy (IX71, Olympus, Japan).

2.3. Sample preparation and the LTRS system

Cells in logarithmic growth phase were made into suspension in PBS prior to Raman measurement. Then the Raman spectra of single living cells were recorded using a home-made LTRS system. Figure 1 briefly illustrated the working mechanisms of the LTRS system used in this study. Diode laser beam with 785 nm (LE-LS-785-XXRaman, StarBright Laser AB, Sweden) was firstly collimated with a spatial filter to achieve a beam diameter of approximately 6 mm. Then, the laser beam was spectrally filtered using a band pass filter and finally delivered into an inverted microscope (IX71, Olympus, Japan) equipped with a 100 × oil immersion objective with a numerical aperture of 1.3 through a dichroic mirror.

Biomedical Optics EXPRESS

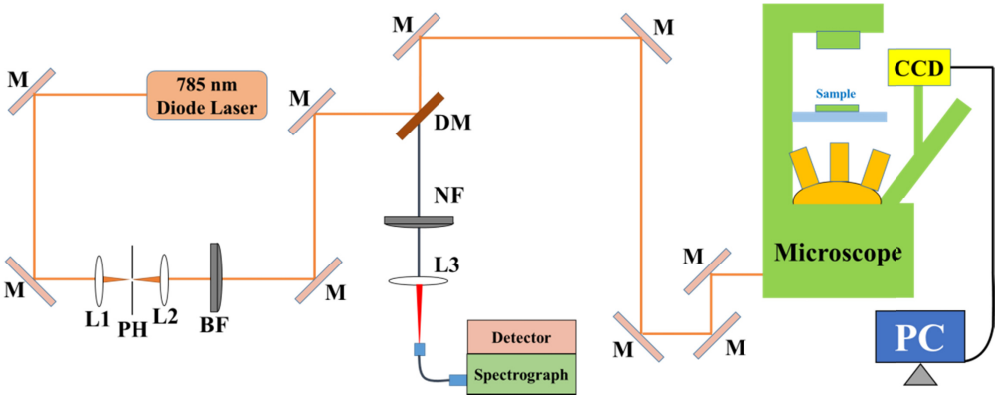

Fig. 1. Schematic of the home-made laser tweezers Raman spectroscopy (LTRS) system. Diode laser beam of 785 nm was delivered to an inverted microscope for both trapping RPE cells and generating Raman signals from cells. Backwards Raman scattering light was recorded by a back-illuminated and deep-depletion near-infrared intensified CCD. M: mirror; L: lens; PH: pinhole; BF: band-pass filter; DM: dichroic mirror; NF: notch filter.

After passing through a sample holder with a quartz bottom (80 μm of thickness) that was placed on the 3D scan stage, the output beam was focused to generate a single beam optical trap. The beam trap was moved to capture the moving cells within samples and the selected cells could be trapped in the laser focus at 20 μm height above the quartz bottom. Meanwhile, the same laser beam was employed to excite Raman scattering for the trapped cell with focus size of 1 μm. Back scattering Raman signal from each cell was collected by the same objective and then directed to reach a charge-coupled device detector (7439-0001, Princeton Instruments, USA), which was cooled to −120 °C in order to reduce the dark current by four optical parts, including a dichroic mirror, a notch filter, lens and a single fiber. The single fiber with 50 μm core diameter could collect and transmit Raman signals to the spectrometer. The end face of the fiber was the equal of 50 μm pinhole, making the optical path of the LTRS system to possess confocal configuration and eliminate the stray light with a great extent. In addition, cells can be illuminated by a white light illumination lamp above the sample holder and images of trapped cells were constantly monitored through a video camera system. On this basis, spectra were recorded with 40 seconds of integration time and 2 mW of laser power from 500 to 1800 cm^{-1} via software package WinSpec32 (Princeton Instruments, USA). Three measurements were carried out for each cell, and an average spectrum of them was used for representing Raman characteristic of each cell. Finally, a total spectrum from 27, 28, and 28 RPE cells for control, oxidative stress, and protective effect groups were acquired respectively.

2.4. Data preprocessing and pattern recognition

All the spectral data preprocessing was performed consistently. An automated algorithm for autofluorescence background removal is firstly applied to the measured raw data to extract pure Raman spectra [29]. Given the state of Micro-Raman system may be different when repeating the experiment, the pure Raman spectra are then normalized according to the area under the curve so as to eliminate the effect of the system.

We implement algorithms of principal components analysis (PCA) and decision trees (DT) from the SPSS software package (version 19.0, IBM, USA) for statistical analysis. Typically, analysis DT model based on classification and regression trees (CRT) generally consists of three steps [30]. First, a maximum tree is built using a binary split-procedure. Although the maximum tree describes training data sets, it is usually overgrown and may result in over-fitting. Hence, the next step is to prune the over-fitting model, resulting in less

Biomedical Optics EXPRESS

complex trees. Finally, the optimal tree is selected using the cross-validation procedure [31]. Such a procedure will further minimize the possibility of over-fitting.

3. Results

3.1 Hydrogen peroxide-induced ROS production and effects on cell viability

Cell viability was assayed in all groups, and the result of the group with hydrogen peroxide intervention was approximately (71.3 ± 4.0)% of the control group, indicating certain damage to the cells. While the group with the combined addition of hydrogen peroxide and ligustrazine, the rate went up to (85.6 ± 0.2)% of the control group which implied that the cells were protected from damage by ligustrazine. It would be useful to know production of ROS so as to determine whether this protective effect is to avoid the oxidative stress of cells. As we know, the generation of ROS could be verified by observation of changes in fluorescent intensity of H2DCFDA resulting from intracellular probe oxidation. To determine whether ROS was involved in the regulation of apoptosis induced by hydrogen peroxide, the fluorescent DCFH-DA product was measured using fluorescence microscopy (Fig. 2(a)). As shown in Fig. 2(b), hydrogen peroxide induced greater production of ROS in RPE cells than that of control cells ($p<0.05$). As the effects of oxidative stress and relative resistant reagent for RPE cells were still unclear and the molecular mechanisms together with characteristic differences for cellular oxidative stress need to be determined. The LTRS method was further performed to explore the spectral characterization of RPE cells and the underlying oxidative mechanism.

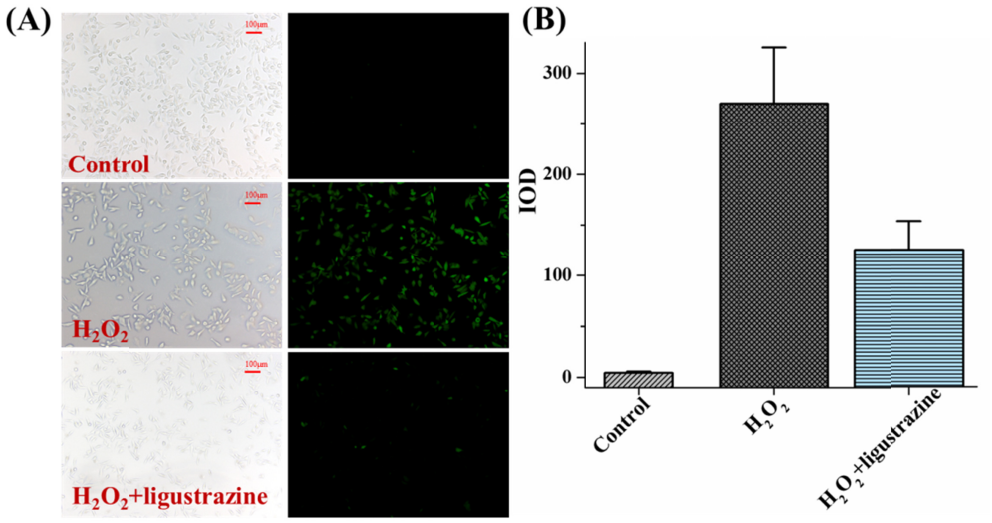

Fig. 2. Measurement of ROS production by fluorescence microscopy. (**A**) Visualization and (**B**) Integral optical density (IOD) value of fluorescent product for different groups.

3.2 Raman spectroscopy of single RPE cells after oxidative stress challenge and the effect of ligustrazine

Representative Raman spectra with high quality are obtained from human RPE cell line before and after oxidative stress challenge. Averaged and normalized spectra are shown in Fig. 3 from pair-comparison among different groups, along with the difference spectra at the bottom of figure. The standard deviations, overlying as shaded color fill in this figure, demonstrated good spectral reproducibility within each group, which guaranteed a better comparison of spectral characteristics among different groups for both peaks assignment analysis and latter statistical analysis. It was difficult to quantify whether differences exist

Biomedical Optics EXPRESS

among these spectra, because these spectra exhibit similar spectral profiles, indicating the same components in cells. Several prominent Raman bands can be consistently observed in cells and then assigned in Table 1 according to previous work [32–36]. Various signals were assigned to nucleic acids, proteins or lipids and provided adequate information to assess variations in spectral characteristics.

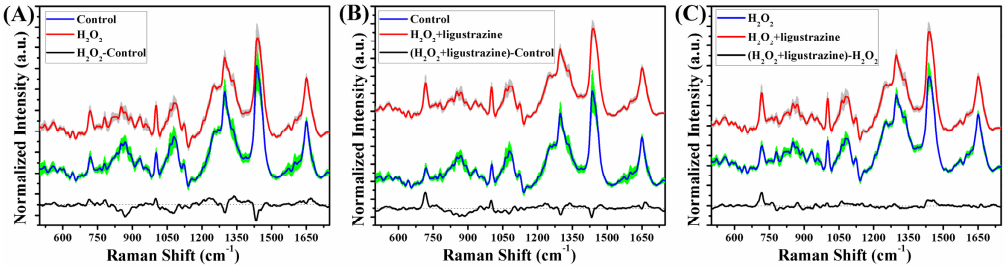

Fig. 3. Pair-comparison of normalized mean Raman spectra from (**A**) the control group and the oxidative stress challenge group, (**B**) the control and ligustrazine group, (**C**) the oxidative stress challenge group and the ligustrazine group. The shaded areas (grey and green) represent the standard deviations of the means. Also shown at the bottom is the difference spectrum.

Table 1. Band positions and assignments of RPE cells from control and oxidative groups

Band (cm^{-1})	Raman Assignment
518	S-S stretching
622	phenylalanine
640	protein: C-C twist, tyrosine
667	G, T
682	G
716	A
744	T
759	T
780	C/U ring breathing
812	DNA: ribosomal protein, tyrosine
832	out of plane ring breathing (tyrosine), DNA: O-P-O stretch
852	tyrosine, protein: C-C skeletal
869	tryptophan, PE, C-C stretching, PC, lipid: CH_2 deformation
891	DNA: phosphodiester and sugar-phosphate backbone, protein: C-C skeletal
932	C-C stretching (proline, valine and protein backbone (α-helix), glycogen)
953	carotenoid, cholesterol
970	lipid: chain C-C
1003	phenylalanine
1062	lipid: skeletal C-C stretch

Biomedical Optics EXPRESS

1078	DNA: O-P-O$^-$
1121	GlcNac
1154	protein: C-C and C-N stretching, carotenoids
1185	T, G
1207	tyrosine, phenylalanine
1254	A, T, amide III
1298	lipid: CH_2 deformation
1333	A, G, protein: C-H deformation
1388	nucleic acid
1436	CH_2 and CH_3 deformation, peptide side chains, phospholipids
1547	A, G
1560	acetyl coenzyme
1574	C = C stretching symmetric (phenylalanine)
1600	C = C in-plane bending (phenylalanine, tyrosine)
1650	amide I
1740	lipid: C = O stretch

Although it is not feasible to quantify the specific value of single band intensity, inverse trends were found at different spectra region. For example, after oxidative stress challenge (Fig. 3(a)), bands located at 716, 759, 1003, and 1650 cm^{-1} tented to have increased intensities, while 891, 1298, and 1436 cm^{-1} showed a decreasing trend, as well as such in Figs. 3(b) and 3(c).

3.3 Multivariate analysis of Raman spectra from RPE cells

We performed PCA to verify significant differences between all three groups. To explore any intimation and reliable markers to discriminate the histological type and oxidative status of the RPE cells, two types of data source were fed into the software package for factor analysis, including whole Raman data and the band data. Since the first two principal components (PCs) contain primary effects and explain the most variance in the PCA process, while the variance explained by PCs>3 gradually decline, using scores and projections of the first two PCs keeps the near original spectral information. In both cases, each group exhibited division with partially overlap with others (Figs. 4(a) and 4(b)). However, a trend in the distribution of these groups can still be identified as shown in the figure. This trend is similar to an arc, starting with the control group, going through the groups with high oxidative stress and last the ligustrazine group, respectively. Moreover, inspection of the loading plots shows that most bands exhibit similar concentrations between whole Raman data and the band data (Figs. 4(c) and 4(d)). These two phenomena suggest the oxidation of hydrogen peroxide-induced stress to cells, but the degree of stress between cells is not the same. Meanwhile, with the additional combination of ligustrazine, the ability of intercellular inhibition is quite different. This results in PC score distribution on the aliasing and trend.

Biomedical Optics EXPRESS

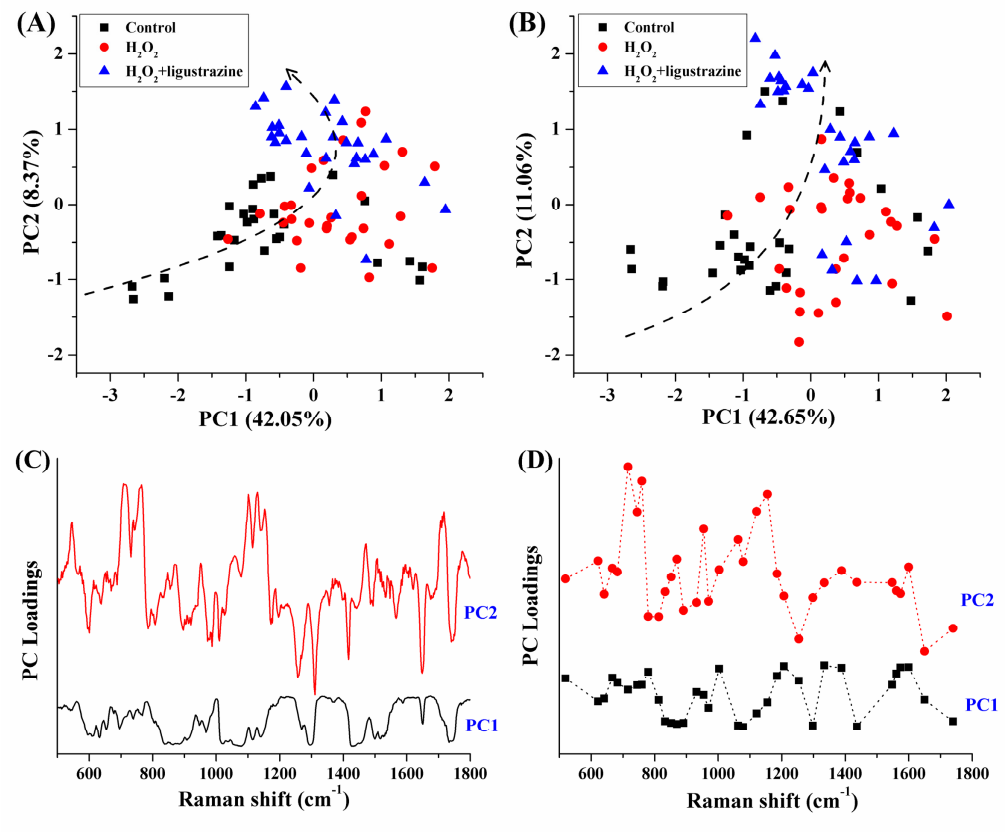

Fig. 4. Score plots of the first two principal components by analysis of (**A**) whole Raman data and (**B**) bands data, along with the loading plots for (**C**) PC1 and (**D**) PC2.

Furthermore, we implement DT model based on CRT algorithm that is a commonly employed statistical classifier using the concept of information entropy. Briefly, at each node of the tree, the CRT algorithm selects one data attribute based on normalized information gain. The normalized information gain is obtained by most effectively splitting its set of samples into subsets. These subsets are enriched in one class or the other. Selection of child-node property is based on the parameter called Gini index and then the property with the lowest Gini index during splitting is selected [37]. Here, we apply Gini index to build the DT model, and a ten-fold cross-validation procedure is used to evaluate the predictive error of the model. As mentioned above, whole Raman data and the band data of cell samples were used to construct relative models by CRT algorithm. The obtained diagnostic sensitivity and specificity were put together in Table 2 for comparison. The classification accuracy of each model was more than 90%, indicating that only a few samples have been misclassified. Moreover, the outcome of each model was not significantly affected by the input data source and the performance of whole spectra and bands as data input were basically the same.

Biomedical Optics EXPRESS

Table 2. Classification by growing method of CRT algorithm based on whole cell Raman data and bands data

Model	Data source	Predicted		
		Accuracy	Sensitivity	Specificity
All three groups	Whole	92.8%	94.6%	100%
	Bands	92.8%	94.6%	100%
Control vs. H_2O_2	Whole	94.5%	89.3%	100%
	Bands	92.7%	85.7%	100%
Control vs. H_2O_2 + ligustrazine	Whole	94.5%	96.4%	92.6%
	Bands	96.4%	96.4%	96.3%
H_2O_2 vs. H_2O_2 + ligustrazine	Whole	94.6%	-	-
	Bands	96.4%	-	-

The band data-based tree illustrates the band importance during the cross-validation procedure. The band importance means a contribution of each band to the establishment of the model as a variable. During cross-validation, the tree quantified the band importance in correct classification. It is important to discover those bands with key roles in classification. Top ten bands with the most importance in each model can be found in Fig. 5. Considering that RPE cells are basically composed of three types of macromolecules (i.e. protein, nucleic acid and lipid), in order to explore characteristic changes of hydrogen peroxide-induced oxidative stress in RPE cells, those important bands were classified based on their assigned biological identities. Subsequently, pairs of the bands were determined according to their assignment results that mainly based on the assignments of same components, chemical bonds (with the same or different vibrational modes), or biological functions. The qualitative and quantitative comparison between these paired bands will continue to be discussed according to the attribution and biological characteristics of these bands.

Biomedical Optics EXPRESS

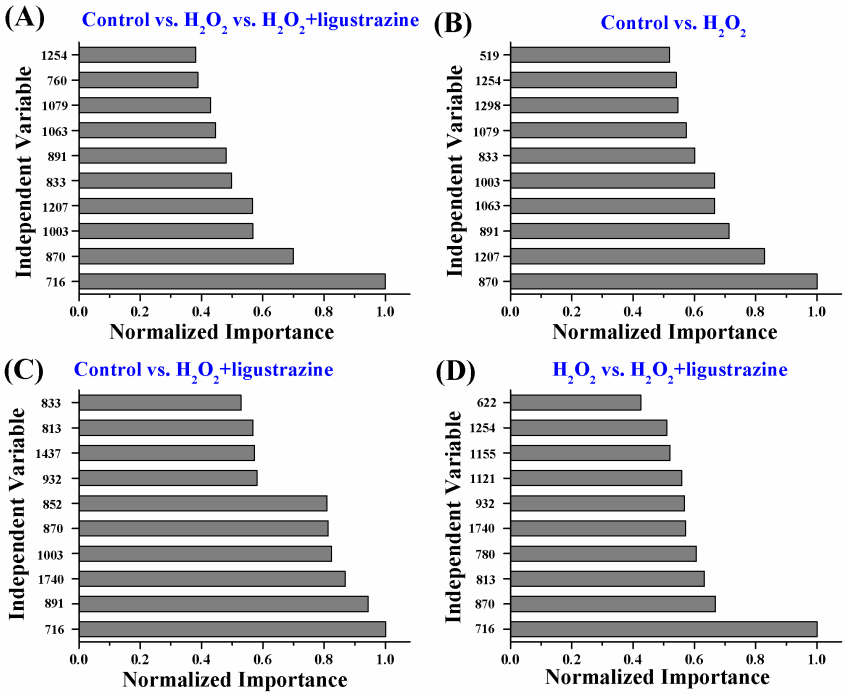

Fig. 5. Importance of independent Raman bands in the CRT models executed for (**A**) all three groups, (**B**) control vs. high oxidative stress, (**C**) control vs. ligustrazine, (**D**) high oxidative stress vs. ligustrazine. The band importance means a contribution of each band to the establishment of the model as a variable.

A simple and effective diagnostic algorithm proposed on the basis of empirical analyses of Raman spectra in terms of peak-intensity-ratio measurements has been applied to a series of biological samples [35,38]. After determining the classification and comparison methods, we summed up all possible changes according to existing knowledge, and the significance of changes are tested by Students' *t*-test analysis, as shown in Fig. 6. It shows very clearly the significant differences (*, $p<0.05$; **, $p<0.01$) between the control group, the oxidation group and the protective group (ligustrazine addition). We found that the difference between the oxidation group and the control group was concentrated in the protein, suggesting that the oxidative stress site was located in some amino acids molecules or vibrational mode. In contrast, the protective group showed four significant changes compared with the control group, less than the oxidation group, but it involved all three macromolecules. Compared with the oxidation group, the relative contents of several protein bands in the control and protective groups showed the same variation trend (i.e. 869/891, 869/932, and 1436/1650). With the addition of ligustrazine, a significant change was only found on one pair of protein band (1254/1650), and the relative content of other protein bands was similar to the control group. Two relative contents from nucleic acid and one of such from lipid also altered significantly (Figs. 6(b) and 6(c)). The data indicated that the effect of ligustrazine on cells was omni-directional, and it was largely different from that of oxidative stress to some extent. The protective effect of ligustrazine can only be achieved by the interaction of a variety of biological molecules.

Biomedical Optics EXPRESS

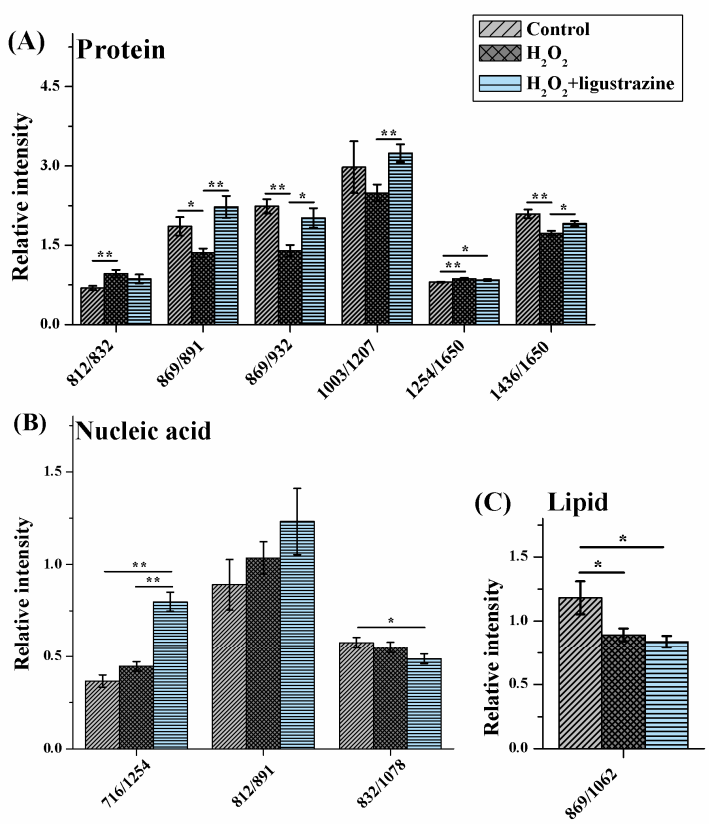

Fig. 6. Relative quantitation of three cellular macromolecules that comes from (**A**) protein, (**B**) nucleic acid, and (**C**) lipid, respectively. X-axis: ratio of Raman bands; *: p<0.05: **: p<0.01.

4. Discussion

Oxidative stress of RPE is an important risk factor in ocular diseases. However, neither the underlying mechanism that is characteristic of oxidative stress for RPE cell has not been deeply investigated nor the oxidation resistant reagent has not been fully clarified. Noninvasive detection of oxidation-induced damages that can clarify early molecular mechanism has been concerned by researchers. Immobilization of cells on a substrate by physical or chemical approaches would perturb cellular biology, and make it difficult to acquire Raman signals of cells above the background generated from the surface [39]. Therefore, in this work, the effects of hydrogen peroxide-induced oxidative stress and the protective effects of ligustrazine on human RPE cells were firstly characterized by using label-free LTRS technique. According to our results, after hydrogen peroxide challenge, the level of ROS in the RPE cells was obviously increased, indicating cell injury. In comparison, the level of ROS of those cells with additional ligustrazine was lower than that of hydrogen peroxide alone. Test of cell viability also confirmed that the applying of ligustrazine increased the cell viability. As shown in single-cell Raman spectroscopy and statistical analysis, the spectral characteristics of three macromolecules from protein, nucleic acid and lipid were further demonstrated at the molecular level.

The results of this work further confirmed that ROS is involved in the cellular signaling pathway and post-translational modification in RPE cells, thus affecting cell growth function [40,41]. Due to hydrogen peroxide, the ability to resist ROS oxidation was impaired, together

Biomedical Optics EXPRESS

with the production of oxidative stress reflected in relative changes of amino acids or vibration modes in protein. For example, the band ratio of 812/832 was significantly increased in the oxidation group, indicating that tyrosine and its internal 'out of plane ring breathing mode' was affected by oxidation. Such interaction also suggested that the molecular vibration of tyrosine was sensitive to oxidation, resulting in structural changes. Interestingly, both bands of 869 and 932 cm^{-1} came from C-C stretching, except that with different protein species. The C-C stretching of 932 cm^{-1} of protein molecules were from proline, valine and protein backbone (α-helix conformation), while 891 cm^{-1} reflected the mode of C-C skeletal. As a result, the ratios of both 869/891 and 869/932 were significantly decreased in the oxidation group. However, after adding ligustrazine, the relative intensity was not different to the control group (Fig. 6), which indicated that hydrogen peroxide changed the content and structure of some amino acids by reaction of ROS with protein, resulting in functional damage of protein [42,43]. It also demonstrated some protective mechanism against these protein damages by ligustrazine. It may involve a variety of metabolic behaviors of cells, including energy metabolism, lipid metabolism, amino acid metabolism, and protein synthesis, etc.

We also noticed about relative contents of amides (1254/1650, amide I vs. amide III) and lipid (869/1062, CH_2 deformation vs. skeletal C-C stretch, Figs. 6(a) and 6(c) were also different from control, and that the addition of ligustrazine did not reverse this trend. The change of band ratio of amides may suggest a desamidization was triggered and resulted in modification of the spatial structure of proteins, and eventually it leaded to loss of protein activity or modification of biological function [44]. Moreover, the lipid is the main component of the cell membrane, which is susceptible to peroxidation induced by ROS, and the product from ROS reaction can cause damage to either the cell membrane or the organelle membrane [45,46]. The failure of ligustrazine to play a protective role in this situation suggested its protection was limited. We also noticed the ligustrazine may affect nucleic acids (716/1254, A vs. A (T); 832/1077, O-P-O stretch vs. $O\text{-}P\text{-}O^-$, Fig. 6(b)). Its effects may involve two aspects, nucleic acid bases (also paired bases) and DNA phosphoric acid skeleton.

In summary, by using the LTRS technique, this work preliminarily discussed the hydrogen peroxide-induced oxidative stress of RPE cells and the anti-oxidation and collateral effects of ligustrazine. The finding helps to better understand the mechanisms of abnormal oxidative stress affecting the RPE, and it also gives insights to develop anti-oxidation drugs for the treatment of eye diseases. This study has its limits that all the experimental results are only achieved from in vitro tissue and current results lack spatial information for RPE cells, and further studies such as in vivo testing and Raman hyperspectral imaging are required.

5. Conclusion

In the present work, we performed label-free detection of hydrogen peroxide-induced oxidative stress and protective effect in human RPE cells using LTRS method. The results demonstrated characteristic alterations of RPE cells after oxidative injury. The ROS level of cells was significantly increased after hydrogen peroxide application, and protein and lipid were significantly affected by the oxidative damage. Cell transduction pathway and protein modification after translation and relative physiological processes were possibly involved according to relative changes of tyrosine and vibration modes in protein. This work has obtained preliminary results on oxidative stress damage and anti-oxidation mechanism of RPE cells in the field of retinopathy. Those findings lay the basis and experimental reference for both understanding the molecular mechanisms underlying oxidative stress and exploiting non-invasive biomarkers for the detection and treatment of retinopathy. Also, imminence requirement to systematically pursue metabolic characteristics should be noted more precisely in the future.

Biomedical Optics EXPRESS

Funding

National Natural Science Foundation of China (81770948); the Fujian Provincial Health System Young and Middle-aged Talents Training Project (2016-ZQN-62); the Scientific Research Talent Training Project of Fujian Provincial Health and Family Planning Commission (2018-1-70); the Startup Science Research Foundation for High-level Talents of Fujian Medical University (XRCZX2017031); and the Startup Fund for Scientific Research of Fujian Medical University (2017XQ1017).

Disclosures

The authors declare that there are no conflicts of interest related to this article.

References

1. O. Strauss, "The retinal pigment epithelium in visual function," Physiol. Rev. **85**(3), 845–881 (2005).
2. A. A. Davis, P. S. Bernstein, D. Bok, J. Turner, M. Nachtigal, and R. C. Hunt, "A human retinal pigment epithelial cell line that retains epithelial characteristics after prolonged culture," Invest. Ophthalmol. Vis. Sci. **36**(5), 955–964 (1995).
3. J. Kopitz, F. G. Holz, E. Kaemmerer, and F. Schutt, "Lipids and lipid peroxidation products in the pathogenesis of age-related macular degeneration," Biochimie **86**(11), 825–831 (2004).
4. J. Cai, K. C. Nelson, M. Wu, P. Sternberg, Jr., and D. P. Jones, "Oxidative damage and protection of the RPE," Prog. Retin. Eye Res. **19**(2), 205–221 (2000).
5. S. Beatty, H. Koh, M. Phil, D. Henson, and M. Boulton, "The role of oxidative stress in the pathogenesis of age-related macular degeneration," Surv. Ophthalmol. **45**(2), 115–134 (2000).
6. J. Hanus, C. Anderson, and S. Wang, "RPE necroptosis in response to oxidative stress and in AMD," Ageing Res. Rev. **24**(Pt B), 286–298 (2015).
7. M. Drobek-Słowik, D. Karczewicz, and K. Safranow, "[The potential role of oxidative stress in the pathogenesis of the age-related macular degeneration (AMD)]," Postepy Hig. Med. Dosw. **61**, 28–37 (2007).
8. M. Farnoodian, C. Halbach, C. Slinger, B. R. Pattnaik, C. M. Sorenson, and N. Sheibani, "High glucose promotes the migration of retinal pigment epithelial cells through increased oxidative stress and PEDF expression," Am. J. Physiol. Cell Physiol. **311**(3), C418–C436 (2016).
9. W. Y. Huang, H. Wu, D. J. Li, J. F. Song, Y. D. Xiao, C. Q. Liu, J. Z. Zhou, and Z. Q. Sui, "Protective effects of blueberry anthocyanins against H_2O_2-induced oxidative injury in human retinal pigment epithelial cells," J. Agric. Food Chem. **66**(7), 1638–1648 (2018).
10. Y. Yan, Y. Ren, X. Li, X. Zhang, H. Guo, Y. Han, and J. Hu, "A polysaccharide from green tea (Camellia sinensis L.) protects human retinal endothelial cells against hydrogen peroxide-induced oxidative injury and apoptosis," Int. J. Biol. Macromol. **115**, 600–607 (2018).
11. G. Liu, C. D. Zhang, J. Wang, and W. C. Jia, "Inhibition of the oxidative stress-induced miR-125b protects glucose metabolic disorders of human retinal pigment epithelium (RPE) cells," Cell. Mol. Biol. **64**(4), 1–5 (2018).
12. F. Jiang, J. Qian, S. Chen, W. Zhang, and C. Liu, "Ligustrazine improves atherosclerosis in rat via attenuation of oxidative stress," Pharm. Biol. **49**(8), 856–863 (2011).
13. R. Fu, Y. Zhang, Y. Guo, Y. Zhang, Y. Xu, and F. Chen, "Digital gene expression analysis of the pathogenesis and therapeutic mechanisms of ligustrazine and puerarin in rat atherosclerosis," Gene **552**(1), 75–80 (2014).
14. L. L. McManus, A. R. Boyd, G. A. Burke, and B. J. Meenan, "Raman spectroscopy of primary bovine aortic endothelial cells: a comparison of single cell and cell cluster analysis," J. Mater. Sci. Mater. Med. **22**(8), 1923–1931 (2011).
15. K. L. Brown, O. Y. Palyvoda, J. S. Thakur, S. L. Nehlsen-Cannarella, O. R. Fagoaga, S. A. Gruber, and G. W. Auner, "Raman spectroscopic differentiation of activated versus non-activated T lymphocytes: an in vitro study of an acute allograft rejection model," J. Immunol. Methods **340**(1), 48–54 (2009).
16. Y. Yu, J. Wang, J. Lin, D. Lin, W. Chen, S. Feng, Z. Huang, Y. Li, H. Huang, H. Shi, and R. Chen, "An optimized electroporation method for delivering nanoparticles into living cells for surface-enhanced Raman scattering imaging," Appl. Phys. Lett. **108**(15), 153701 (2016).
17. R. Smith, K. L. Wright, and L. Ashton, "Raman spectroscopy: an evolving technique for live cell studies," Analyst (Lond.) **141**(12), 3590–3600 (2016).
18. A. T. Harris, M. Garg, X. B. Yang, S. E. Fisher, J. Kirkham, D. A. Smith, D. P. Martin-Hirsch, and A. S. High, "Raman spectroscopy and advanced mathematical modelling in the discrimination of human thyroid cell lines," Head Neck Oncol. **1**(1), 38 (2009).
19. C. Zhang, P. T. Winnard, Jr., S. Dasari, S. L. Kominsky, M. Doucet, S. Jayaraman, V. Raman, and I. Barman, "Label-free Raman spectroscopy provides early determination and precise localization of breast cancer-colonized bone alterations," Chem. Sci. (Camb.) **9**(3), 743–753 (2018).
20. Y. Yu, J. Lin, D. Lin, S. Feng, W. Chen, Z. Huang, H. Huang, and R. Chen, "Leukemia cells detection based on electroporation assisted surface-enhanced Raman scattering," Biomed. Opt. Express **8**(9), 4108–4121 (2017).

Biomedical Optics EXPRESS

21. K. Chen, Y. Qin, F. Zheng, M. Sun, and D. Shi, "Diagnosis of colorectal cancer using Raman spectroscopy of laser-trapped single living epithelial cells," Opt. Lett. **31**(13), 2015–2017 (2006).
22. S. Ahlawat, A. Chowdhury, A. Uppal, N. Kumar, and P. K. Gupta, "Use of Raman optical tweezers for cell cycle analysis," Analyst (Lond.) **141**(4), 1339–1346 (2016).
23. J. W. Chan, "Recent advances in laser tweezers Raman spectroscopy (LTRS) for label-free analysis of single cells," J. Biophotonics **6**(1), 36–48 (2013).
24. J. W. Chan, D. S. Taylor, and D. L. Thompson, "The effect of cell fixation on the discrimination of normal and leukemia cells with laser tweezers Raman spectroscopy," Biopolymers **91**(2), 132–139 (2009).
25. S. Y. Li, Y. H. Jia, W. G. Sun, Y. Tang, G. S. An, J. H. Ni, and H. T. Jia, "Stabilization of mitochondrial function by tetramethylpyrazine protects against kainate-induced oxidative lesions in the rat hippocampus," Free Radic. Biol. Med. **48**(4), 597–608 (2010).
26. X. Xu, L. Hang, B. Huang, Y. Wei, S. Zheng, and W. Li, "Efficacy of ethanol extract of fructus lycii and its constituents lutein/zeaxanthin in protecting retinal pigment epithelium cells against oxidative stress: in vivo and in vitro models of age-related macular degeneration," J. Ophthalmol. **2013**, 862806 (2013).
27. J. G. Pastorino and J. B. Hoek, "Ethanol potentiates tumor necrosis factor-alpha cytotoxicity in hepatoma cells and primary rat hepatocytes by promoting induction of the mitochondrial permeability transition," Hepatology **31**(5), 1141–1152 (2000).
28. Y. Huang, G. Xu, Y. Peng, S. Chen, and Y. Wu, "Photodynamic effects of ZnPcS(4)-BSA in human retinal pigment epithelium cells," J. Ocul. Pharmacol. Ther. **25**(3), 231–238 (2009).
29. J. Zhao, H. Lui, D. I. McLean, and H. Zeng, "Automated autofluorescence background subtraction algorithm for biomedical Raman spectroscopy," Appl. Spectrosc. **61**(11), 1225–1232 (2007).
30. L. Breiman, J. H. Friedman, R. A. Olshen, and C. J. Stone, "Classification and regression trees," Wadsworth Publishing, Monterey, 218–256 (1983).
31. Y. Chen, Y. Su, L. Ou, C. Zou, and Z. Chen, "Classification of nasopharyngeal cell lines (C666-1, CNE2, NP69) via Raman spectroscopy and decision tree," Vib. Spectrosc. **80**, 24–29 (2015).
32. H. Yao, Z. Tao, M. Ai, L. Peng, G. Wang, B. He, and Y. Li, "Raman spectroscopic analysis of apoptosis of single human gastric cancer cells," Vib. Spectrosc. **50**(2), 193–197 (2009).
33. P. Crow, B. Barrass, C. Kendall, M. Hart-Prieto, M. Wright, R. Persad, and N. Stone, "The use of Raman spectroscopy to differentiate between different prostatic adenocarcinoma cell lines," Br. J. Cancer **92**(12), 2166–2170 (2005).
34. A. G. Shen, Y. Ye, J. W. Zhang, X. H. Wang, J. M. Hu, W. Xie, and J. Shen, "Screening of gastric carcinoma cells in the human malignant gastric mucosa by confocal Raman microspectroscopy," Vib. Spectrosc. **37**(2), 225–231 (2005).
35. M. D. Mannie, T. J. McConnell, C. Xie, and Y. Q. Li, "Activation-dependent phases of T cells distinguished by use of optical tweezers and near infrared Raman spectroscopy," J. Immunol. Methods **297**(1-2), 53–60 (2005).
36. K. Hamada, K. Fujita, N. I. Smith, M. Kobayashi, Y. Inouye, and S. Kawata, "Raman microscopy for dynamic molecular imaging of living cells," J. Biomed. Opt. **13**(4), 044027 (2008).
37. L. Ou, Y. Chen, Y. Su, C. Zou, and Z. Chen, "Detection of genomic DNA damage from radiated nasopharyngeal carcinoma cells via surface-enhanced Raman spectroscopy (SERS)," Appl. Spectrosc. **70**(11), 1821–1830 (2016).
38. C. Yu, E. Gestl, K. Eckert, D. Allara, and J. Irudayaraj, "Characterization of human breast epithelial cells by confocal Raman microspectroscopy," Cancer Detect. Prev. **30**(6), 515–522 (2006).
39. Z. Tao, G. Wang, X. Xu, Y. Yuan, X. Wang, and Y. Li, "Monitoring and rapid quantification of total carotenoids in Rhodotorula glutinis cells using laser tweezers Raman spectroscopy," FEMS Microbiol. Lett. **314**(1), 42–48 (2011).
40. R. G. Allen and M. Tresini, "Oxidative stress and gene regulation," Free Radic. Biol. Med. **28**(3), 463–499 (2000).
41. M. Valko, D. Leibfritz, J. Moncol, M. T. Cronin, M. Mazur, and J. Telser, "Free radicals and antioxidants in normal physiological functions and human disease," Int. J. Biochem. Cell Biol. **39**(1), 44–84 (2007).
42. E. R. Stadtman, "Protein oxidation in aging and age-related diseases," Ann. N. Y. Acad. Sci. **928**(1), 22–38 (2001).
43. M. J. Davies, "The oxidative environment and protein damage," Biochim. Biophys. Acta **1703**(2), 93–109 (2005).
44. P. Pacher, J. S. Beckman, and L. Liaudet, "Nitric oxide and peroxynitrite in health and disease," Physiol. Rev. **87**(1), 315–424 (2007).
45. S. X. Zhang, J. J. Wang, A. Dashti, K. Wilson, M. H. Zou, L. Szweda, J. X. Ma, and T. J. Lyons, "Pigment epithelium-derived factor mitigates inflammation and oxidative stress in retinal pericytes exposed to oxidized low-density lipoprotein," J. Mol. Endocrinol. **41**(3), 135–143 (2008).
46. R. Kohen and A. Nyska, "Oxidation of biological systems: oxidative stress phenomena, antioxidants, redox reactions, and methods for their quantification," Toxicol. Pathol. **30**(6), 620–650 (2002).